

Population Pharmacokinetic-Pharmacodynamic Model of the Vascular-Disrupting Agent 5,6-Dimethylxanthenone-4-Acetic Acid in Cancer Patients

Jing Li,¹ Michael B. Jameson,² Bruce C. Baguley,³ Roberto Pili,¹ and Sharyn D. Baker¹

Abstract Purpose: To develop a population pharmacokinetic-pharmacodynamic (PK-PD) model that defines the dose-concentration-effect relationship of 5,6-dimethylxanthenone-4-acetic acid (DMXAA), using plasma 5-hydroxyindole-3-acetic acid (5-HIAA) as a biomarker for the antivasular effect of DMXAA.

Experimental Design: The plasma DMXAA and 5-HIAA concentration data were obtained from 124 patients receiving DMXAA monotherapy as a 20-minute i.v. infusion weekly or every 3 weeks at doses of 6 to 4,900 mg/m². The PK and PD data were analyzed by nonlinear mixed effects modeling with NONMEM version 5.

Results: DMXAA concentration-time profiles were well described by a three-compartment model with saturable elimination (Michaelis-Menten kinetics). Body surface area (BSA) and sex were significant covariates on the volume of distribution of the central compartment (V_1) and the maximum elimination rate (V_m), respectively. Population estimates for V_m , K_m (concentration at which half V_m is achieved), and V_1 were $112[1 + 0.474(2 - \text{sex})]$ $\mu\text{mol/L/h}$, 102 $\mu\text{mol/L}$, and $8.19(\text{BSA}/1.8)^{0.857}$ liters, respectively (sex in V_m is equal to 1 for males and equal to 2 for females). The effect of DMXAA on plasma 5-HIAA was described by the stimulatory E_{max} model, where population estimates for baseline, E_{max} , and EC_{50} were 46.3 $\mu\text{mol/L}$, 2.62-fold increase of the baseline value, and 631 $\mu\text{mol/L}$, respectively.

Conclusions: DMXAA plasma disposition is characterized by a saturable elimination process. BSA-guided dosing is important. The present PK-PD model, with 5-HIAA as a biomarker, supports the use of DMXAA doses of 1,000 to 2,000 mg/m² in phase II studies, and provides an example of how PK-PD models can be used to aid in selection of drug doses for phase II evaluation.

5,6-Dimethylxanthenone-4-acetic acid (DMXAA) is a small-molecule vascular-disrupting agent that selectively disrupts established tumor blood vessels. It has been evaluated as monotherapy in phase I trials (1–3) and is being assessed in phase II trials in combination with cytotoxic agents. Recent data from a phase II study have shown that the combination of DMXAA with carboplatin and paclitaxel increased survival by 5.2 months in patients with non-small cell lung cancer compared with treatment with carboplatin and paclitaxel alone (median survival 14 versus 8.8 months; ref. 4).

DMXAA induces rapid vascular collapse and subsequent tumor hemorrhagic necrosis through induction of apoptosis in

tumor vascular endothelial cells (5) and indirect vascular effects involving various cytokines, in particular, tumor necrosis factor- α , serotonin, and nitric oxide (6–10). DMXAA has also shown an antiangiogenesis effect *in vivo* (11). The degree of DMXAA-induced tumor hemorrhagic necrosis is significantly correlated with increased tumor vascular permeability, decreased functioning tumor blood vessels, and increased plasma 5-hydroxyindoleacetic acid (5-HIAA) concentrations (as a measure of serotonin release; ref. 7). Serotonin, a naturally occurring vasoactive substance that is released from platelets into plasma under various pathologic conditions, is involved in the antitumor and host effects of DMXAA and also mediates the effects of tumor necrosis factor- α (9). Serotonin plasma concentrations increase in response to DMXAA in mice (8), suggesting that it might be a surrogate marker for antivasular effects. However, serotonin is unstable during blood processing and storage, whereas its primary metabolite, 5-HIAA, has greater stability and accumulates in plasma following serotonin release (12). Phase I studies have shown that 5-HIAA plasma concentrations increased in a dose-dependent manner at DMXAA doses of ≥ 650 mg/m² (2, 3). Therefore, 5-HIAA, providing an index of vascular damage, could be a suitable surrogate biomarker for the antivasular and/or antitumor effects of DMXAA.

One challenge in the clinical development of molecularly targeted therapies is to identify an optimal biological and

Authors' Affiliations: ¹The Sidney Kimmel Comprehensive Cancer Center at Johns Hopkins, Baltimore, Maryland; ²Waikato Hospital, Hamilton, New Zealand; and ³Auckland Cancer Society Research Center, University of Auckland, Auckland, New Zealand

Received 6/14/07; revised 12/20/07; accepted 1/3/08.

Grant support: Antisoma PLC (London, United Kingdom).

The costs of publication of this article were defrayed in part by the payment of page charges. This article must therefore be hereby marked *advertisement* in accordance with 18 U.S.C. Section 1734 solely to indicate this fact.

Requests for reprints: Jing Li, Barbara Ann Karmanos Cancer Institute, Wayne State University, 4100 John R, HWCRC/Room 523, Detroit, MI 48201. Phone: 313-576-8258; E-mail: lijn@karmanos.org.

©2008 American Association for Cancer Research.

doi:10.1158/1078-0432.CCR-07-1475

Table 1. Patient demographic and baseline characteristics

	United Kingdom study	New Zealand study	DART study	All studies
Sex (male/female)*	23/23	21/42	12/3	56/68
Age (y)	58 (34-77)	54 (24-75)	51 (27-69)	56 (24-77)
Weight (kg)	65 (45-88)	73.1 (39.7-131.5)	72 (50-90)	70 (40-131)
Height (m)	1.68 (1.49-1.85)	1.66 (1.48-1.86)	1.64 (1.51-1.78)	1.65 (1.48-1.86)
BSA (m ²)	1.75 (1.40-2.15)	1.85 (1.40-2.30)	1.80 (1.43-2.01)	1.80 (1.40-2.30)
WHO performance status †				
0	13 (0.28)	13 (0.21)	6 (0.40)	32 (0.26)
1	29 (0.63)	22 (0.35)	8 (0.53)	59 (0.47)
2	4 (0.09)	28 (0.44)	1 (0.07)	33 (0.27)
3	0	0	0	0
4	0	0	0	0
Total bilirubin (μmol/L)	11 (6-20)	6 (2-20)	7 (4-21)	8 (2-21)
ALT (IU/L)	23 (10-99)	19 (6-322)	25 (11-176)	22 (6-322)
AST (IU/L)	31 (16-143)	26 (5-295)	26 (12-75)	26 (5-295)
Alk phos	100 (52-1191)	107 (13-948)	100 (37-1125)	107 (13-1191)
Serum creatinine (μmol/L)	82 (57-167)	80 (60-120)	80 (45-170)	80 (45-170)
Serum albumin (g/L)	39 (29-51)	37 (22-43)	42 (32-50)	38 (22-51)
Hemoglobin (g/L)	119 (95-150)	114 (88-151)	124 (94-151)	116 (88-151)

NOTE: Data are presented as median (range).
Abbreviations: ALT, alanine aminotransferase; AST, aspartate aminotransferase; Alk phos, alkaline phosphatase.
*Values are patient numbers.
† Values are shown as patient number (probability).

efficacious dose that may be below the maximum tolerated dose. Defining dose-concentration-effect relationships could aid in this process. Population pharmacokinetic-pharmacodynamic (PK-PD) analysis using nonlinear mixed effects modeling is particularly useful to characterize the dose-concentration-effect relationship for new chemical entities or established drugs because it allows simultaneous analysis of PK (concentration) and PD (effect) data from all complete or incomplete individual data sets as well as identification of sources of interindividual PK-PD variability.

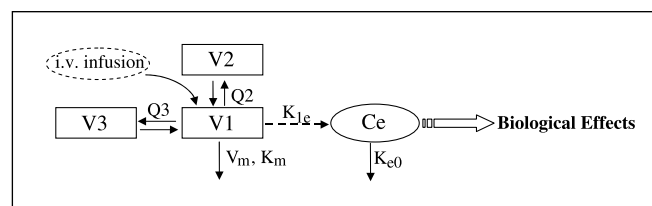
The purpose of this study was to develop a population PK-PD model to (a) characterize DMXAA plasma concentration-time profiles following single- and multiple-dose administration in cancer patients treated with single-agent DMXAA, (b) relate the plasma concentration-time profiles to changes in 5-HIAA concentrations as a biomarker for antivasular effect, and (c) identify clinical covariates that influence DMXAA pharmacokinetics and pharmacodynamics. In addition, simulations were done to show how the model can be used to predict the antivasular effect and guide dose selection for future studies of DMXAA.

Materials and Methods

Clinical studies and patients. The clinical and pharmacokinetic data used in the analysis were obtained from three phase I studies involving a total of 124 cancer patients treated with single-agent DMXAA as previously described (1-3). Patients with histologically confirmed solid tumors that were not amenable to any standard therapy or were refractory to conventional therapy were eligible for participation in the trials. Patient demographic and baseline clinical characteristics including sex, age, weight, height, body surface area (BSA), WHO performance status, liver function (i.e., total bilirubin, alanine aminotransferase, aspartate aminotransferase, and alkaline phosphatase), kidney function (i.e., serum creatinine), serum albumin, and hemoglobin are listed in

Table 1. There were no clinically significant differences in patient demographic and clinical characteristics across the three studies. The study protocols were approved by the medical ethics committee in all study centers, and written informed consent was obtained from all the patients.

Two parallel phase I dose escalation studies composed of (a) a two-center study in the United Kingdom with patients receiving DMXAA once weekly and (b) a single-center study in New Zealand with patients receiving DMXAA once every 3 weeks. The drug was given as 20-minute i.v. infusion in both studies. The starting dose was 6 mg/m², and at least three patients were treated at each dose level. In the United Kingdom trial, 15 dose levels (i.e., 6, 10.2, 20.4, 40.8, 81.6, 160, 320, 500, 650, 1,000, 1,300, 1,750, 2,300, 3,700, and 4,900 mg/m²) were evaluated in 46 patients. One course of treatment consisted of 6 weekly infusions, and a maximum of two courses (12 infusions) was permitted. In the New Zealand trial, 19 dose levels (i.e., 6, 10.2, 20.4, 40.8, 81.6, 160, 240, 320, 500, 650, 850, 1,100, 1,375, 1,650, 2,000, 2,600, 3,100, 3,700, and 4,900 mg/m²) were assessed in 63 patients. One course of treatment consisted of one infusion of DMXAA every 3 weeks, with a maximum of six courses (six infusions) in patients with stable disease, but where a tumor response occurred, a patient could continue for two courses following maximum response. The third trial, the DART study, was a phase I multicenter double-blind randomized six-way inpatient dose-ranging crossover safety study to further characterize the effect of DMXAA on QT_c interval, ophthalmic safety, and pharmacodynamic



Scheme 1. Effect compartment PK-PD model.

effects on tumor blood flow that was assessed by using dynamic contrast enhanced magnetic resonance imaging. In this study, 15 patients were randomly allocated to a treatment sequence according to multiple six-by-six Latin squares and were blinded to receive each of six doses (i.e., 300, 600, 1,200, 1,800, 2,400, and 3,000 mg/m²) at weekly intervals. Patients who derived clinical benefit from the course of six infusions were offered additional courses of weekly infusion for 6 weeks at 1,200 mg/m² and allowed to remain on treatment until they no longer had clinical benefit or disease progression, or until toxicity led to patient withdrawal.

PK and PD data. A total of 3,050 DMXAA plasma concentration-time data were obtained from 124 patients treated with single-agent DMXAA in the three studies. In the United Kingdom study, blood samples were collected before the infusion; immediately at the end of infusion; and at 0.25, 0.5, 0.75, 1, 1.5, 2, 4, 8, 12, and 24 h after the first infusion on week 1. Additional blood samples were drawn before the infusion, immediately at the end of infusion, and 4 h after the infusion in the subsequent treatment on week 2 and beyond. In the New Zealand study, blood samples were collected before the infusion; 10 min before the end of infusion; immediately at the end of infusion; and at 0.25, 0.5, 0.75, 1, 1.5, 2, 4, 8, 12, and 24 h after the first infusion on week 1 (and, in one patient at each dose level, repeated with the second infusion on week 4), and additional samples were obtained before the infusion, at the end of infusion, and 4 h after the infusion in the subsequent treatment.

In the DART study, blood samples were taken before the infusion; immediately at the end of infusion; and at 1, 2, 4, 8, 12, and 24 h after each infusion.

All blood samples were centrifuged at 1,300 × g for 10 min (for the United Kingdom and New Zealand studies) or at 1,200 × g for 5 min (for the DART study), and aliquots of plasma were stored at -70°C (United Kingdom and DART studies) or -20°C (New Zealand study) until analysis. DMXAA plasma concentrations were determined using validated high-performance liquid chromatography methods with fluorescence detection (for United Kingdom and New Zealand studies; ref. 2) or with tandem mass spectrometric detection (liquid chromatography/tandem mass spectrometry, for the DART study; ref. 3).

Blood samples for 5-HIAA plasma concentrations were taken at the same time as above for DMXAA concentrations, and 5-HIAA concentrations were determined by high-performance liquid chromatography with electrochemical detection (12).

Population PK analysis. DMXAA and 5-HIAA concentration-time data were analyzed using the nonlinear mixed effects modeling approach as implemented in NONMEM (version 5; University of California, San Francisco, CA). All analyses were done with the first-order approximation method. Xpose 3.1/S-PLUS 6.0 was used for graphical diagnostics and covariate screen. The population PK model of DMXAA was developed in two steps: (a) basic (structural) model development and (b) covariate model development.

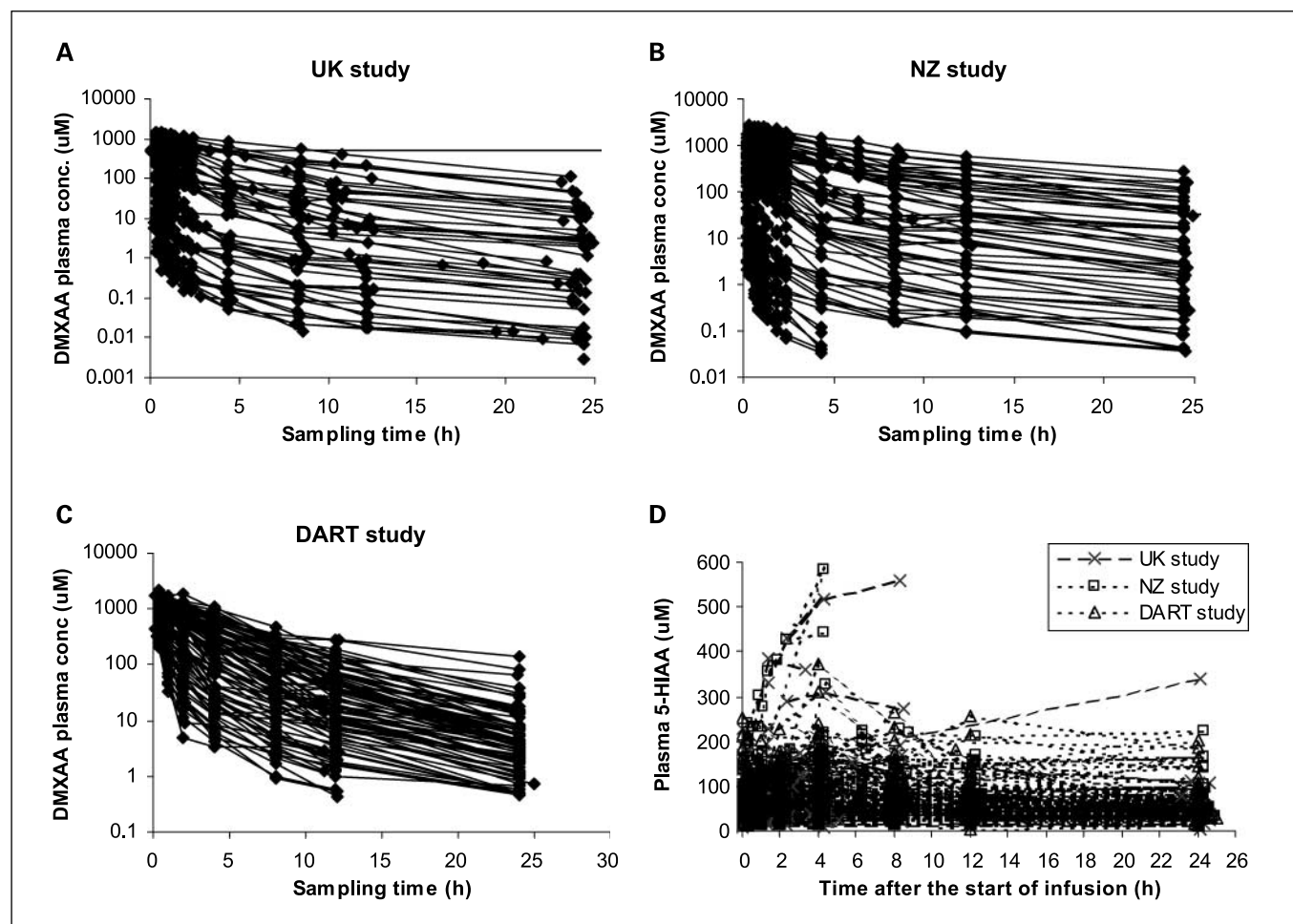


Fig. 1. Observed DMXAA plasma concentration-time profiles following single-dose administration in the (A) United Kingdom, (B) New Zealand, and (C) DART studies. D, observed plasma 5-HIAA concentration-time profiles following each i.v. infusion of DMXAA in individual patients from all three studies.

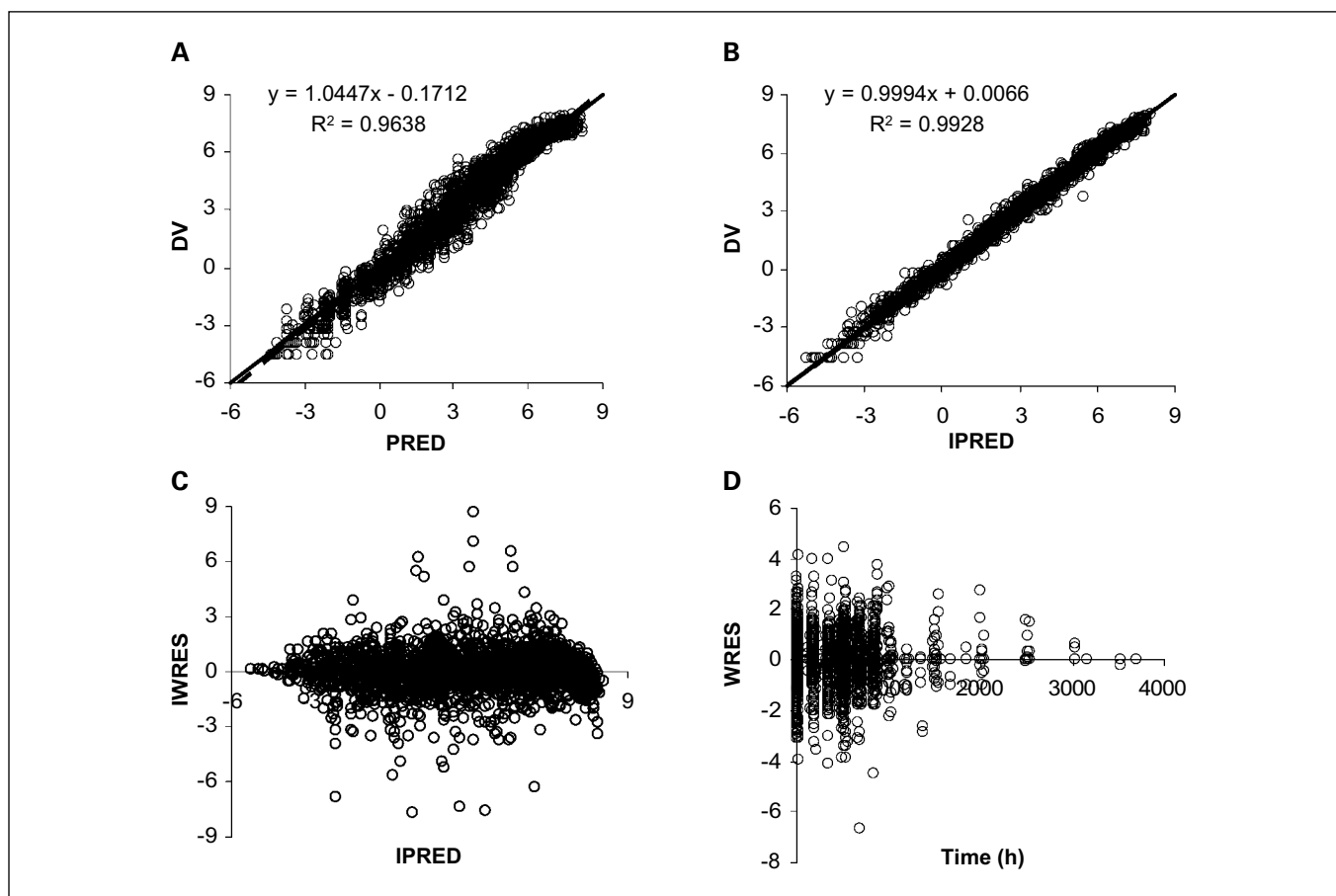


Fig. 2. Basic goodness-of-fit plots from the final PPK three-compartment model with Michaelis-Menten elimination and with sex and BSA being introduced as a significant covariate on V_m and V_d , respectively. Drug input is actual dose (mg/h). DV, observed concentrations (log transformed); PRED, population predicted concentrations (log transformed); IPRED, individual predicted concentrations (log transformed); IWRES, individual weighted residues; WRES, weighted residues.

The structural model was built to fit multiple-dose DMXAA plasma concentration-time profiles from all 124 patients simultaneously. DMXAA concentration data were log transformed. Three-compartment models with first-order elimination or nonlinear elimination characterized by Michaelis-Menten kinetics (Eq. A) were tested to fit DMXAA plasma concentration data.

$$R = \frac{V_m \times C}{K_m + C} \quad (\text{A})$$

where R is the elimination rate, V_m is the maximum elimination rate, K_m is the concentration at which half-maximum elimination rate is achieved, and C is DMXAA plasma concentration.

Mean population PK variables, interindividual variability, and residual error (intraindividual variability) were assessed in the model. Interindividual variability for each PK variable was modeled with an exponential function. Residual error was modeled with a combination method, including an additive and a proportional part, each of which could be excluded if it was estimated to be negligible. Individual PK variables were obtained by posterior Bayesian estimation.

Model selection for nonhierarchical models (i.e., linear and nonlinear elimination models) was guided by graphical goodness-of-fit plots (e.g., observed versus predicted plasma concentrations, residuals versus predicted concentrations, and weighted residuals versus predicted concentration), Akaike information criterion (AIC), and precision of estimates. AIC was calculated as $\text{AIC} = (-2\text{LL}) + 2 \times p$, where -2LL is the NONMEM objective function value (OFV, $-2 \log$

likelihood) and p is the number of PK variables. The model was chosen on the basis of smaller values of AIC, better precision of estimates, and superior goodness-of-fit plots.

The covariate model building was a stepwise process. A screen for potential significant covariates was done using S-PLUS 6.2/Xpose 3.1 software (Uppsala University, Uppsala, Sweden) with generalized additive model (GAM; ref. 13). The potential covariates, as listed in Table 1, as well as the treatment cycle and bioanalysis assay were tested for influence on the structural PK variables. When a covariate value was missing in a patient, this covariate value was replaced by the population median value. The frequency of missing covariate was $<10\%$. The potential significant covariates selected from GAM analysis were introduced into the covariate model as linear, exponential, or power function, and assessed in the PPK models. Discrimination between hierarchical models was made by comparison of the NONMEM OFV and by visual inspection of the goodness-of-fit plots. The difference between the OFV for two hierarchical models is approximately χ^2 distributed, where the degrees of freedom are based on the difference between the numbers of estimated variables. A significant covariate was selected to be retained in the final model if addition of the covariate resulted in a decrease in OFV >3.875 ($P < 0.05$) during the forward full covariate model building, and removal of the covariate resulted in an increase in OFV >10.828 ($P < 0.001$) during the stepwise backward model reduction. In addition, the increase in precision of the variable estimate (% relative SE of prediction) and reduction in interindividual variability were used as another indicator of the improvement of the goodness of fit.

Population PK-PD analysis. Plasma 5-HIAA was used as a biomarker for the antivasular effect of DMXAA. Because the increase in 5-HIAA plasma concentration in each patient lagged behind the plasma concentration time course of DMXAA, an effect compartment model, which assumes the rate of drug distribution to and from the hypothetical effect site will determine the rate of onset of effect, was implemented to relate DMXAA concentrations to the change of plasma 5-HIAA (Scheme 1; refs. 14, 15). In such a model, the time course of the effect site concentration (C_e) is described by the rate constant k_{e0} from the effect compartment; following the dose of the drug, there is a slow accretion of the drug response that is governed by the inhibition or stimulation of factors controlling this response. This can produce either a decrease or increase in the observed response variable (such as a biomarker) depending on whether the input or disposition process is inhibited or stimulated (14). The vascular-disrupting effect of DMXAA resulted in an increase of 5-HIAA, and therefore, a stimulatory effect compartment model was chosen and different functional forms (i.e., linear, E_{max} and sigmoidal E_{max}) were tested. A stimulatory E_{max} model related to baseline (Eq. B) was found to best describe the relationship between the effect site concentration of DMXAA and 5-HIAA.

$$E = E_0 \left(1 + \frac{E_{max} \times C_e}{EC_{50} + C_e} \right) \quad (B)$$

where E is the observed effect at the corresponding effect-site concentration (C_e); and E_0 , E_{max} , and EC_{50} represent baseline, maximum effect (times of baseline), and concentration at half-maximum effect, respectively.

DMXX and 5-HIAA concentration-time data were fitted with the model simultaneously using the first-order approximation method as implemented in NONMEM, with population PK variables fixed to the previously obtained values from the final PK model. Interindividual variability for each PK and PD variable was modeled as an exponential function. An additive error model was used because DMXAA concentration and 5-HIAA concentration data were log transformed in the data file, enabling an additive error model, which approximates to a proportional error model on untransformed data. The covariate PD model building was done as described above.

Simulations. To illustrate the use of the model for dose selection, the concentration-time courses of plasma DMXAA and 5-HIAA, as predicted by the final PK-PD model, were simulated under different dose levels ranging from 50 to 4,400 mg/m² in a typical subject. This is a hypothetical individual who had PK and PD values equal to population median values and covariate values equal to the median values of the studied group, unless otherwise stated.

Results

Structural PK model. Figure 1 shows the observed individual DMXAA plasma concentration-time profiles following single- and multiple-dose administration in all patients enrolled to the three trials. DMXAA plasma concentration-time profiles following a 20-minute i.v. infusion were characterized by a tri-exponential decline by visual inspection (Fig. 1). Therefore, a three-compartment model with a first-order elimination process from the central compartment was first tested to fit DMXAA plasma concentration data. However, the linear-elimination model generally overpredicted the observed concentrations at lower drug dose levels (e.g., dose <100 mg/m²), whereas it underpredicted the observed concentrations at higher dose level (e.g., dose >1,750 mg/m²), as shown in the goodness-of-fit plots and individual observed and predicted DMXAA concentration-time curves (data not shown).

The prediction bias suggested that DMXAA disposition might exhibit a nonlinear PK behavior over the studied dose levels (from 6 to 4,900 mg/m²), and therefore, a three-compartment

Table 2. Population PK and PD variables of DMXAA, expressed as the estimate (with % relative SE of estimation), and the corresponding interindividual variability

Covariate	Structural PK model*	Final PK-PD model
	None	$V_m = \theta_1 [1 + \theta_{10} (1 - \text{sex})]$; $V_1 = \theta_2 (BSA / 1.8)^{0.11}$
OFV	-2,383	-2,532
TV V_m ($\mu\text{mol/L/h}$)	241 (12)	165 [†] (22)
TV V_1 (liters)	7.39 (3.6)	8.19 [‡] (3.1)
TV V_2 (liters)	5.59 (15)	13.2 (8.7)
TV V_3 (liters)	26.1 (8.7)	52.4 (8.3)
TV Q_2 (L/h)	7.08 (13)	5.15 (63)
TV Q_3 (L/h)	3.28 (10)	2.33 (18)
TV K_m ($\mu\text{mol/L}$)	183 (14)	102 (26)
$\theta_{8,\S}$	0.274 (5.7)	0.275 (4.5)
$\theta_{9,\parallel}$	0.0412 (67)	0.0318 (43)
θ_{10}	—	0.474 (46)
θ_{11}	—	0.857 (37)
IIV of V_m (%)	41 (22)	43 (23)
IIV of V_1 (%)	32 (19)	26 (20)
IIV of V_2 (%)	77 (21)	56 (23)
IIV of V_3 (%)	68 (21)	97 (92)
IIV of Q_2 (%)	56 (33)	49 (19)
IIV of Q_3 (%)	62 (30)	69 (40)
IIV of K_m (%)	41 (37)	13 (290)
BL ($\mu\text{mol/L}$)	—	46.3 (5.8)
E_{max} (folds of baseline)	—	2.62 (34)
EC_{50} ($\mu\text{mol/L}$)	—	631 (58)
K_{e0} (h^{-1})	—	0.331 (36)
IIV of BL (%)	—	51 (20)
IIV of E_{max} (%)	—	30 (66)
IIV of EC_{50} (%)	—	59 (100)
IIV of K_{e0} (%)	—	84 (50)

Abbreviations: TV, typical value; V_m , maximum elimination; V_1 , volume of distribution of the central compartment; V_2 , volume of distribution of peripheral compartment 1; V_3 , volume of distribution of peripheral compartment 2; Q_2 and Q_3 , intercompartment clearance; K_m , drug concentration at which half-maximum elimination rate is achieved; IIV, interindividual variability (% CV); BL, baseline plasma 5-HIAA concentration; E_{max} , maximum increase of plasma 5-HIAA concentration; EC_{50} , DMXAA concentration at effect site to achieve 50% of the E_{max} ; K_{e0} , first-order rate constant from the effect compartment to biological effect.

*The structural model is a three-compartment model with Michaelis-Menten elimination from the central compartment. Drug input is actual dose (mg/h).

[†]Typical value for the male, calculated from V_m ($\mu\text{mol/L/h}$) = $112(1 + 0.474(2 - \text{sex}))$, male: sex = 1, female: sex = 2.

[‡]Typical value for those with BSA of 1.8 m², calculated from V_1 (liters) = $8.19(BSA/1.8)^{0.857}$, the median value of BSA is 1.8 m².

[§]Additive component in residue error model.

^{||}Proportional component in residue error model.

model with a nonlinear elimination process characterized by Michaelis-Menten kinetics (Eq. A) from the central compartment was tested to fit DMXAA concentration data. The nonlinear model resulted in a reduction in the NONMEM OFV by 1,275 and a corresponding drop in the AIC by 1,269, compared with the linear model. In addition, the goodness-of-fit plots and individual observed and predicted concentration-time curves (data not shown) did not show any prediction bias

from the nonlinear model. Therefore, the three-compartment model with Michaelis-Menten elimination from the central compartment was chosen as the structural PK model.

Covariate PK model. The following potentially significant covariates that were selected from GAM analysis were included and tested during the covariate model building: sex on V_m , BSA on V_1 , sex on V_2 , BSA and assay on V_3 , BSA on Q_2 , height on Q_3 , and age on K_m . Sex and BSA were identified as two significant covariates. With sex being added as the significant covariate on VM, the OFV was decreased by 49 ($P < 0.001$) from the structural model, and the further addition of BSA on V_1 resulted in a further decrease of OFV by 100 ($P < 0.001$). Further additions of sex on V_2 , BSA and assay on V_3 , BSA on Q_2 , height on Q_3 , or age on K_m either resulted in a negligible improvement in the fitting (with the decrease in OFV < 3.875 , $P > 0.05$) or extreme difficulty in the model convergence. Therefore, the final PK model consisted of a three-compartment model with nonlinear elimination, with sex and BSA being included as a significant covariate on V_m and V_1 , respectively. Figure 2 shows the goodness-of-fit plots from the final PK model. The population-predicted and posterior Bayes (individual)-predicted DMXAA concentrations were highly correlated with the observed values, with correlation coefficients (r^2) of 0.9455 and 0.9825, respectively (Fig. 2); IWRES versus IPRED plots and individual observed and predicted concentration-time profiles (data not shown) indicated no prediction bias.

The typical population PK variables and respective interindividual variability estimated from the structural and final PK models are presented in Table 2.

From the structural to final model, the value of OFV decreased by 149; however, the addition of covariates sex on V_m [as V_m ($\mu\text{mol/L/h}$) = $112(1+0.474(2-\text{sex}))$, male: sex = 1, female: sex = 2] and BSA on V_1 [as V_1 (liters) = $8.19(\text{BSA}/1.8)^{0.857}$] accounted for small proportion of unexplained interindividual variability on V_m and V_1 (Table 2), suggesting that other clinical covariates that were not tested in the present study may account for a larger proportion of the interindividual variability. For a male with BSA of 1.8 m^2 , the typical population PK variables were estimated from the final model as V_m 165 $\mu\text{mol/L/h}$; K_m 102 $\mu\text{mol/L}$; V_1 8.19 liters; V_2 13.2 liters; V_3 52.4 liters; Q_2 5.15 L/h; and Q_3 2.33 L/h (Table 2).

PK-PD model. The observed plasma 5-HIAA concentration-time profiles following each i.v. infusion of DMXAA in the individual patients are depicted in Fig. 1D. 5-HIAA peak concentrations, in general, appeared between 4 and 12 hours following DMXAA i.v. infusion (Fig. 1D), whereas DMXAA peak concentrations occurred at the end of infusion (20 minutes after the start of infusion). The effect delay was characterized by a first-order rate constant (k_{e0}) of 0.331 per hour (corresponding to a lag time of 3 hours) from the central plasma compartment to an effect compartment. The goodness-of-fit plots for the analysis of plasma 5-HIAA concentration

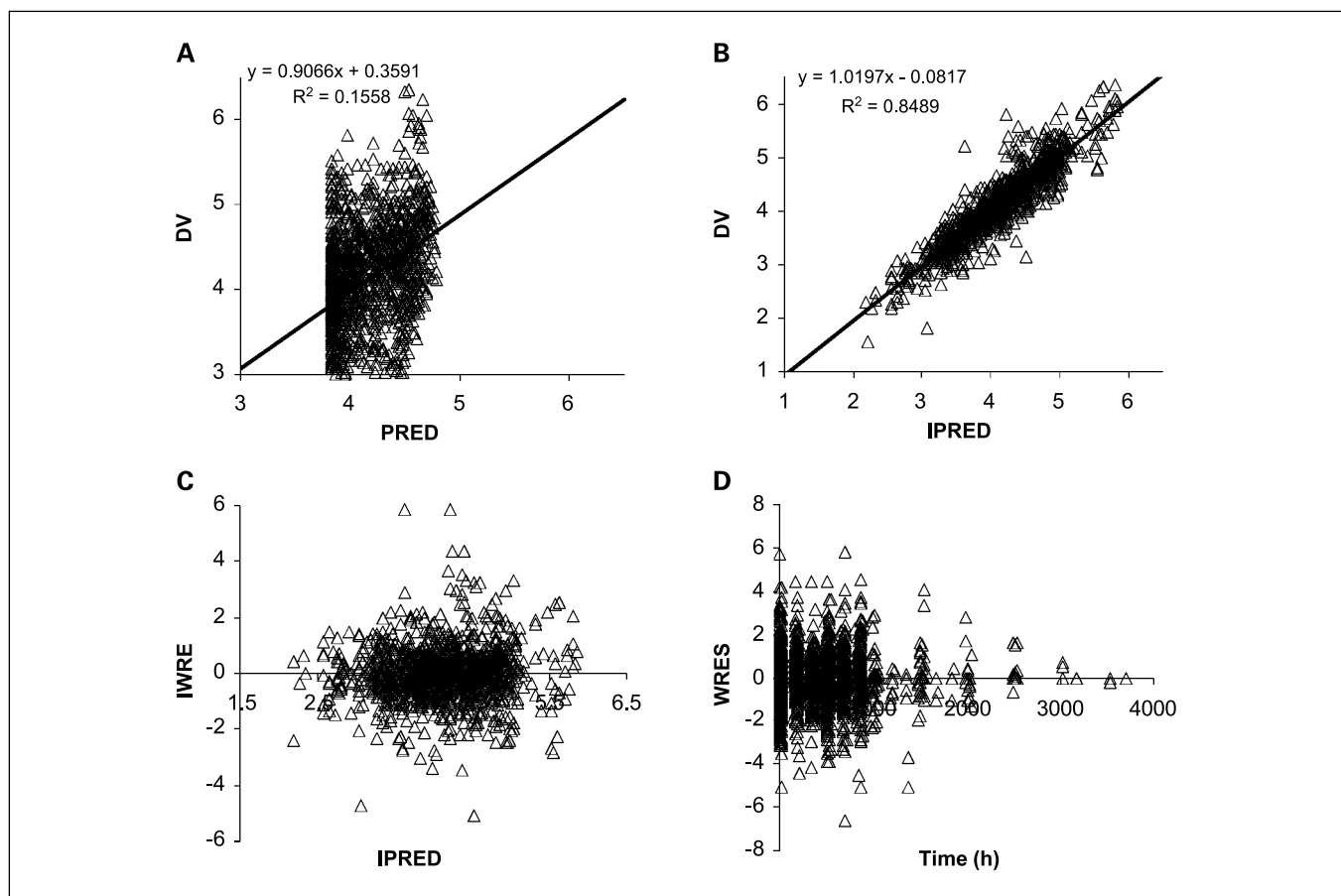


Fig. 3. Basic goodness-of-fit plots from the effect compartment PK-PD analysis of plasma 5-HIAA concentrations. PRED, population predicted concentrations (log transformed).

(PD) data are presented in Fig. 3. The typical population PD variables and their interindividual variability, with percent relative SE of estimation, are shown in Table 2. The population estimates for baseline 5-HIAA plasma concentration (E_0), maximum increase of 5-HIAA (E_{max}), DMXAA concentration resulting in half-maximum effect (EC_{50}) were 46.3 $\mu\text{mol/L}$, 2.62-fold of the baseline value, and 631 $\mu\text{mol/L}$, respectively; the respective interindividual variability was estimated as 51%, 30%, and 59% (Table 2). GAM analyses indicated no significant correlations between any of clinical covariates (listed in Table 1) and PD variables.

Predictions from the final model. The simulated concentration-time curves of DMXAA and 5-HIAA are shown in Fig. 4A and B. With a dose increase from 50 to 4,400 mg/m^2 , the predicted peak plasma DMXAA concentration (C_{max}) at the end of infusion was increased from 27.3 to 2,902 $\mu\text{mol/L}$, which resulted in a peak plasma 5-HIAA concentration increasing from 1.02- to 2.42-fold of the baseline value. The plots of DMXAA dose against peak plasma DMXAA and 5-HIAA concentrations are shown in Fig. 4C. The EC_{50} of DMXAA could be achieved at a dose of $\sim 1,000 \text{ mg/m}^2$.

Discussion

Preliminary analysis from the phase I study data suggested that DMXAA exhibited dose-dependent PK behavior, which was characterized by a nonlinear increase of the area under the concentration-time curve (AUC) and maximum plasma concentration (C_{max}) and decrease of system clearance, with an increase of DMXAA dose in cancer patients (2, 16). The nonlinear PK profile of DMXAA was confirmed and well described by the present population PK model incorporating a three-compartment model with saturable elimination characterized by Michaelis-Menten kinetics.

The nonlinear elimination of DMXAA could be attributable to its saturable metabolism. DMXAA is extensively metabolized, mainly through acyl glucuronidation catalyzed by UDP-glucuronosyltransferase 1A9 and 2B7 (17) and through 6-methylhydroxylation by cytochrome P450 1A2 (CYP1A2; refs. 18–21). *In vitro* enzyme kinetic studies have shown that in human liver microsomes, the mean apparent K_m values are 143 and 21 $\mu\text{mol/L}$, respectively, for acyl glucuronidation and 6-methylhydroxylation, and the respective mean apparent V_m values are 0.71 and 0.04 nmol/min/mg (22). The K_m value of 102 $\mu\text{mol/L}$ estimated from the population PK model was in line with the K_m value of 143 $\mu\text{mol/L}$ for DMXAA glucuronidation determined in human microsomes, indicating that glucuronidation was a predominant and rate-limited pathway for DMXAA elimination from the body.

The population PK model suggested that the maximum elimination rate (V_m) of DMXAA was sex dependent: Males had higher V_m than females. This result was consistent with previous animal studies that showed that DMXAA exhibited a higher system clearance in male rats than in female rats (23). The sex-dependent DMXAA elimination could be due to gender-dependent expression and/or activity of metabolic enzymes responsible for the metabolism of DMXAA, in particular CYP1A2 and UGT1A9 and 2B7. It has been reported that CYP1A2 activity is greater in males than females (24) and that mRNA expression and activity of UDP-glucuronosyltransferases can be regulated by sex hormones (25, 26).

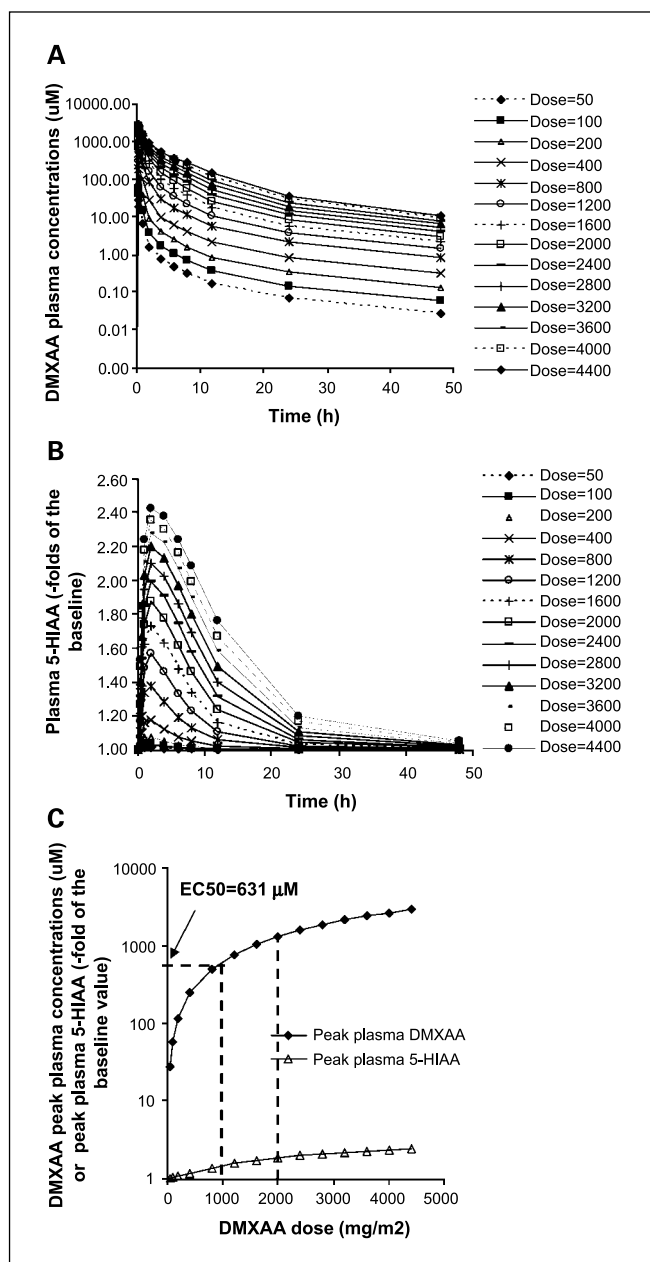


Fig. 4. Simulated time course of DMXAA (A) and 5-HIAA (B) plasma concentrations, from the final population PK-PD model in a typical male individual who has population median values of PK and PD variables and clinical covariates. C, the plots of DMXAA doses against peak DMXAA and 5-HIAA plasma concentrations.

The combined addition of sex and BSA as significant covariates in the PK model reduced the NONMEM OFV by 149 ($P < 0.001$); nevertheless, they accounted for a small fraction of the interindividual variability in DMXAA pharmacokinetics (Table 2), suggesting that other covariates that were not evaluated in this study may make a larger contribution to the PK variability and should be further investigated. Factors influencing DMXAA metabolic pathways could alter the total elimination rate and contribute significantly to the interindividual PK-PD variability of the drug. Genetic polymorphisms in the metabolic enzymes have potential clinical significance. UGT1A9, UGT2B7, and CYP1A2 polymorphisms have been

repeatedly reported to be associated with altered pharmacokinetics and/or toxicity of a number of compounds such as irinotecan, SN-38, carvedilol, and caffeine (27–31). The evaluation of polymorphisms in UGT1A9, 2B7, and CYP1A2 may account for a significant fraction of the interindividual PK variability of DMXAA. In addition, UGT1A9 and UGT2B7 are inducible by various compounds such as BNF (32), *t*-butylhydroquinone, and 2,3,7,8-tetrachlorodibenzo-*p*-dioxin (33), whereas CYP1A2 can be induced by smoking (34) and certain antitumor agents such as aminoflavone (35). Potential enzyme induction or inhibition by concomitant drugs may alter the pharmacokinetics of DMXAA when it is combined with other chemotherapeutic agents and should be further investigated in the future phase II/III combination studies.

DMXAA-induced increase of plasma 5-HIAA concentrations has been shown to be a result of its vascular effects involving the release of serotonin by platelets, and therefore, 5-HIAA was used as a biomarker of DMXAA treatment. The time courses of plasma DMXAA and 5-HIAA concentrations were simultaneously fitted by the effect compartment PK-PD model with a stimulatory E_{\max} model related to baseline describing the antivasular effect of DMXAA. Because of the nonlinearity of DMXAA pharmacokinetics and its E_{\max} effect on plasma 5-HIAA, the increase of 5-HIAA plasma concentration was not proportional to the increase of DMXAA dose. As shown by simulations in a typical individual (Fig. 4C), at a dose of $\sim 1,000$ mg/m², the EC₅₀ (typical population value, 631 μ mol/L) of DMXAA was

achieved at the end of infusion, which resulted in a peak plasma 5-HIAA concentration at ~ 1.45 -fold of the baseline value. When the dose was increased to 2,000 mg/m², DMXAA peak plasma concentration was $\sim 1,300$ μ mol/L and the achieved 5-HIAA peak concentration was ~ 1.87 -fold of the baseline value (Fig. 4). With further increases of the doses beyond 2,000 mg/m², both DMXAA and 5-HIAA peak plasma concentrations gradually increased and reached the plateau (Fig. 4C), whereas DMXAA-induced toxicities (grades 1–4) increased significantly (1, 2). Transient prolongation of the corrected cardiac Q_T interval was observed in all 13 patients evaluated at doses of 2,000 mg/m² and above in the New Zealand study (1) and the maximum tolerated dose of DMXAA was established at 3,700 mg/m² (2). Therefore, combining the pharmacodynamic effect based on the present PK-PD model and toxicity data, a DMXAA dose ranging from 1,000 to 2,000 mg/m² is recommended for future studies, supporting the DMXAA doses of 1,200 and 1,800 mg/m² currently under evaluation in combination with chemotherapy in phase II studies.

In conclusion, DMXAA plasma disposition was characterized by a nonlinear elimination process. BSA was a significant covariate in the PK model, supporting the current use of BSA-guided dosing. The PK-PD model, with 5-HIAA as a biomarker, supports the use of DMXAA dose of 1,000 to 2,000 mg/m² in phase II studies, and provides an example of how PK-PD models can be used to aid in selection of drug doses for phase II evaluation.

References

- Jameson MB, Thompson PI, Baguley BC, et al. Clinical aspects of a phase I trial of 5,6-dimethylxanthenone-4-acetic acid (DMXAA), a novel antivasular agent. *Br J Cancer* 2003;88:1844–50.
- Rustin GJ, Bradley C, Galbraith S, et al. 5,6-Dimethylxanthenone-4-acetic acid (DMXAA), a novel antivasular agent: phase I clinical and pharmacokinetic study. *Br J Cancer* 2003;88:1160–7.
- McKeage MJ, Fong P, Jeffery M, et al. 5,6-Dimethylxanthenone-4-acetic acid in the treatment of refractory tumors: a phase I safety study of a vascular disrupting agent. *Clin Cancer Res* 2006;12:1776–84.
- Pawel V. Update on survival in a phase Ib/2 study of DMXAA (AS1404) combined with carboplatin and paclitaxel in non-small-cell lung cancer (NSCLC). In: AACR-NCI-EORTC; 2006. p. (Abstract 40).
- Ching LM, Cao Z, Kieda C, Zwain S, Jameson MB, Baguley BC. Induction of endothelial cell apoptosis by the antivasular agent 5,6-dimethylxanthenone-4-acetic acid. *Br J Cancer* 2002;86:1937–42.
- Ching LM, Goldsmith D, Joseph WR, Korner H, Sedgwick JD, Baguley BC. Induction of intratumoral tumor necrosis factor (TNF) synthesis and hemorrhagic necrosis by 5,6-dimethylxanthenone-4-acetic acid (DMXAA) in TNF knockout mice. *Cancer Res* 1999;59:3304–7.
- Zhao L, Ching LM, Kestell P, Kelland LR, Baguley BC. Mechanisms of tumor vascular shutdown induced by 5,6-dimethylxanthenone-4-acetic acid (DMXAA): increased tumor vascular permeability. *Int J Cancer* 2005;116:322–6.
- Baguley BC, Zhuang L, Kestell P. Increased plasma serotonin following treatment with flavone-8-acetic acid, 5,6-dimethylxanthenone-4-acetic acid, vinblastine, and colchicine: relation to vascular effects. *Oncol Res* 1997;9:55–60.
- Baguley BC, Cole G, Thomsen LL, Li Z. Serotonin involvement in the antitumor and host effects of flavone-8-acetic acid and 5,6-dimethylxanthenone-4-acetic acid. *Cancer Chemother Pharmacol* 1993;33:77–81.
- Moilanen E, Thomsen LL, Miles DW, Happerfield DW, Knowles RG, Moncada S. Persistent induction of nitric oxide synthase in tumours from mice treated with the anti-tumour agent 5,6-dimethylxanthenone-4-acetic acid. *Br J Cancer* 1998;77:426–33.
- Cao Z, Baguley BC, Ching LM. Interferon-inducible protein 10 induction and inhibition of angiogenesis *in vivo* by the antitumor agent 5,6-dimethylxanthenone-4-acetic acid (DMXAA). *Cancer Res* 2001;61:1517–21.
- Kestell P, Zhao L, Jameson MB, Stratford MR, Folkes LK, Baguley BC. Measurement of plasma 5-hydroxyindoleacetic acid as a possible clinical surrogate marker for the action of antivasular agents. *Clin Chim Acta* 2001;314:159–66.
- Jonsson EN, Karlsson MO. Xpose—an S-PLUS based population pharmacokinetic/pharmacodynamic model building aid for NONMEM. *Comput Methods Programs Biomed* 1999;58:51–64.
- Dayneka NL, Garg V, Jusko WJ. Comparison of four basic models of indirect pharmacodynamic responses. *J Pharmacokinet Biopharm* 1993;21:457–78.
- Cleton A, de Greef HJ, Edelbroek PM, Voskuyl RA, Danhof M. Application of a combined “effect compartment/indirect response model” to the central nervous system effects of tiagabine in the rat. *J Pharmacokinet Biopharm* 1999;27:301–23.
- Jameson MB, Baguley BC, Kestell P, et al. Pharmacokinetics of 5,6-dimethylxanthenone-4-acetic acid (AS1404), a novel vascular disrupting agent, in phase I clinical trial. *Cancer Chemother Pharmacol* 2007;59:681–7.
- Miners JO, Valente L, Lillywhite KJ, et al. Preclinical prediction of factors influencing the elimination of 5,6-dimethylxanthenone-4-acetic acid, a new anticancer drug. *Cancer Res* 1997;57:284–9.
- Zhou S, Paxton JW, Tingle MD, Kestell P. Identification of the human liver cytochrome P450 isoenzyme responsible for the 6-methylhydroxylation of the novel anticancer drug 5,6-dimethylxanthenone-4-acetic acid. *Drug Metab Dispos* 2000;28:1449–56.
- Webster LK, Ellis AG, Kestell P, Rewcastle GW. Metabolism and elimination of 5,6-dimethylxanthenone-4-acetic acid in the isolated perfused rat liver. *Drug Metab Dispos* 1995;23:363–8.
- Kestell P, Paxton JW, Rewcastle GW, Dunlop I, Baguley BC. Plasma disposition, metabolism and excretion of the experimental antitumor agent 5,6-dimethylxanthenone-4-acetic acid in the mouse, rat and rabbit. *Cancer Chemother Pharmacol* 1999;43:323–30.
- Zhou S, Kestell P, Baguley BC, Paxton JW. Preclinical factors influencing the relative contributions of Phase I and II enzymes to the metabolism of the experimental anti-cancer drug 5,6-dimethylxanthenone-4-acetic acid. *Biochem Pharmacol* 2003;65:109–20.
- Zhou S, Kestell P, Baguley BC, Paxton JW. Preclinical factors affecting the interindividual variability in the clearance of the investigational anti-cancer drug 5,6-dimethylxanthenone-4-acetic acid. *Biochem Pharmacol* 2003;65:1853–65.
- Zhou S, Kestell P, Tingle MD, Paxton JW. Gender differences in the metabolism and pharmacokinetics of the experimental anticancer agent 5,6-dimethylxanthenone-4-acetic acid (DMXAA). *Cancer Chemother Pharmacol* 2002;49:126–32.
- Parkinson A, Mudra DR, Johnson C, Dwyer A, Carroll KM. The effects of gender, age, ethnicity, and liver cirrhosis on cytochrome P450 enzyme activity in human liver microsomes and inducibility in cultured human hepatocytes. *Toxicol Appl Pharmacol* 2004;199:193–209.
- Matsumoto J, Yokota H, Yuasa A. Developmental increases in rat hepatic microsomal UDP-glucuronosyltransferase activities toward xenoestrogens and decreases during pregnancy. *Environ Health Perspect* 2002;110:193–6.
- Shibata N, Matsumoto J, Nakada K, Yuasa A, Yokota H. Male-specific suppression of hepatic microsomal UDP-glucuronosyl transferase activities toward sex hormones in the adult male rat administered bisphenol A. *Biochem J* 2002;368:783–8.
- Girard H, Villeneuve L, Court MH, et al. The novel

- UGT1A9 intronic 1399 polymorphism appears as a predictor of 7-ethyl-10-hydroxycamptothecin glucuronidation levels in the liver. *Drug Metab Dispos* 2006;34:1220–8.
28. Carlini LE, Meropol NJ, Bever J, et al. UGT1A7 and UGT1A9 polymorphisms predict response and toxicity in colorectal cancer patients treated with capecitabine/irinotecan. *Clin Cancer Res* 2005;11:1226–36.
29. Gagne JF, Montminy V, Belanger P, Journault K, Gaucher G, Guillemette C. Common human UGT1A polymorphisms and the altered metabolism of irinotecan active metabolite 7-ethyl-10-hydroxycamptothecin (SN-38). *Mol Pharmacol* 2002;62:608–17.
30. Takekuma Y, Takenaka T, Kiyokawa M, et al. Contribution of polymorphisms in UDP-glucuronosyltransferase and CYP2D6 to the individual variation in disposition of carvedilol. *J Pharm Pharm Sci* 2006;9:101–12.
31. Chen X, Wang L, Zhi L, et al. The G-113A polymorphism in CYP1A2 affects the caffeine metabolic ratio in a Chinese population. *Clin Pharmacol Ther* 2005;78:249–59.
32. Meech R, Mackenzie PI. Structure and function of uridine diphosphate glucuronosyltransferases. *Clin Exp Pharmacol Physiol* 1997;24:907–15.
33. Munzel PA, Schmohl S, Heel H, Kalberer K, Bock-Hennig BS, Bock KW. Induction of human UDP glucuronosyltransferases (UGT1A6, UGT1A9, and UGT2B7) by *t*-butylhydroquinone and 2,3,7,8-tetrachlorodibenzo-*p*-dioxin in Caco-2 cells. *Drug Metab Dispos* 1999;27:569–73.
34. van der Weide J, Steijns LS, van Weelden MJ. The effect of smoking and cytochrome P450 CYP1A2 genetic polymorphism on clozapine clearance and dose requirement. *Pharmacogenetics* 2003;13:169–72.
35. Kuffel MJ, Schroeder JC, Pobst LJ, et al. Activation of the antitumor agent aminoflavone (NSC 686288) is mediated by induction of tumor cell cytochrome P450 1A1/1A2. *Mol Pharmacol* 2002;62:143–53.